Solvent Engineering Synthesis of Layered SnO for High-Performance Anodes

Sonia Jaśkaniec[a,b,*], Seán R. Kavanagh[b,c,d,e], Joao Coelho[a,b], Seán Ryan[a,b], Christopher Hobbs[b,f], Aron Walsh[d,e,g,h], David O. Scanlon[c,e,h,i] and Valeria Nicolosi[a,b,*]

[a]School of Chemistry, Trinity College Dublin, Dublin 2, Ireland
[b]CRANN&AMBER, Trinity College Dublin, Dublin 2, Ireland
[c]Department of Chemistry, University College London, 20 Gordon Street, London WC1H 0AJ, UK
[d]Department of Materials, Imperial College London, Exhibition Road, London SW7 2AZ, UK
[e]Thomas Young Centre, University College London, Gower Street, London WC1E 6BT, UK
[f]School of Physics, Trinity College Dublin, Dublin 2, Ireland
[g]Department of Materials Science and Engineering, Yonsei University, Seoul 03722, Korea
[h]The Faraday Institution, Quad One, Harwell Science and Innovation Campus, Didcot, UK
[i]Diamond Light Source Ltd., Diamond House, Harwell Science and Innovation Campus, Didcot, Oxfordshire OX11 0DE, UK

metels@tcd.ie, nicolov@tcd.ie

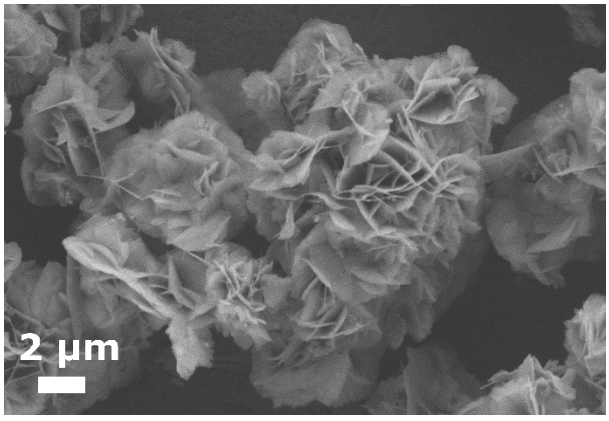

Supplementary Figure 1 SEM micrograph of the SnO produced in a 1L flask.

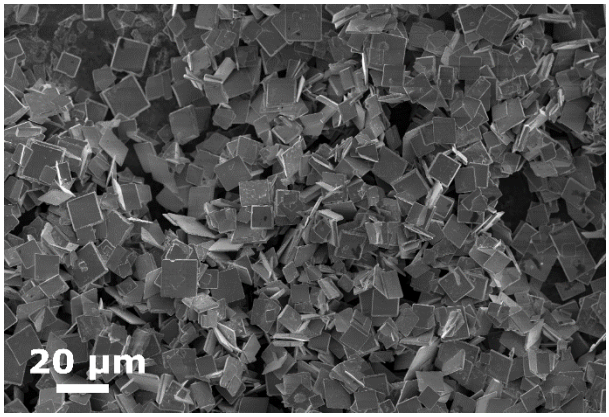

Supplementary Figure 2 SEM micrograph of SnO particles produced in water.

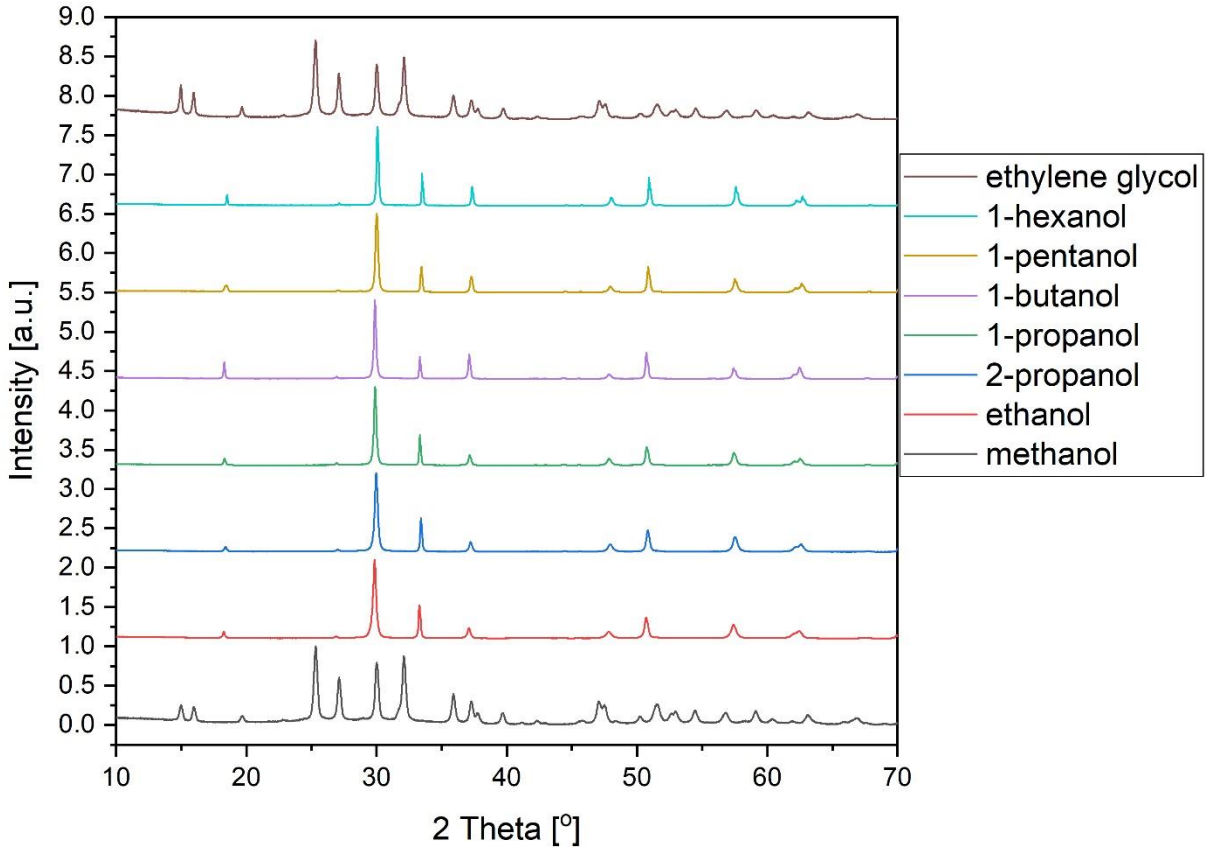

Supplementary Figure 3 Powder XRD of the SnO nanoparticles produced in pure alcohols.

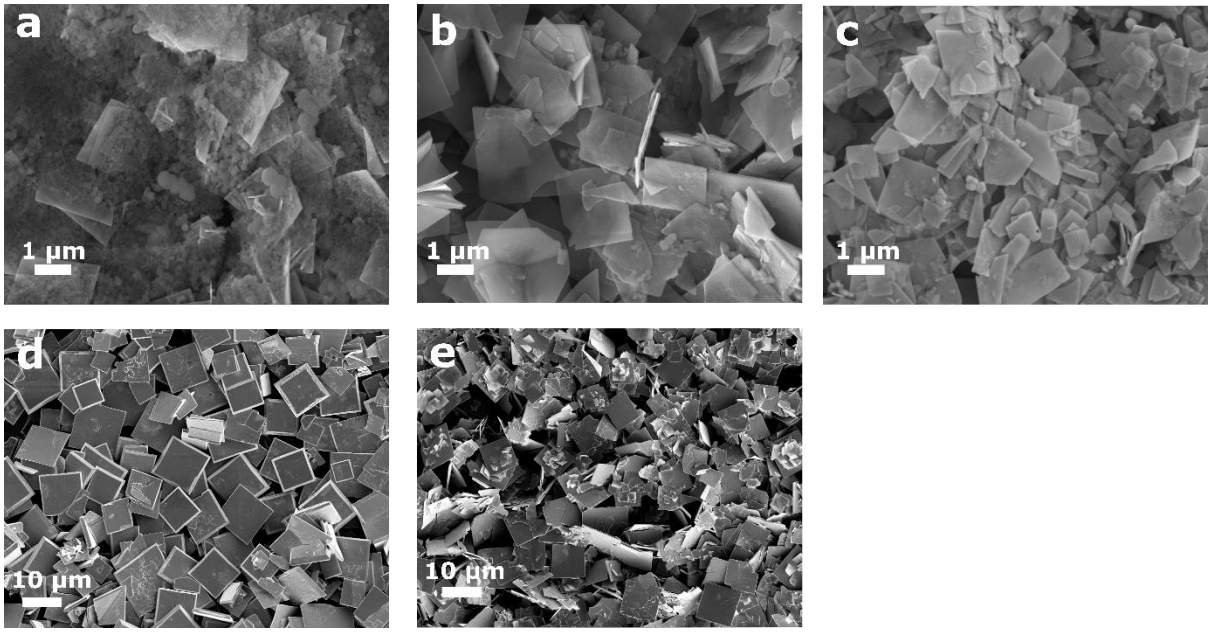

Supplementary Figure 4 SEM micrograph of the SnO samples produced in the methanol:water mixtures in the ratio a) 90:10, b) 80:20, c) 60:40, d) 40:60 and e) 20:80.

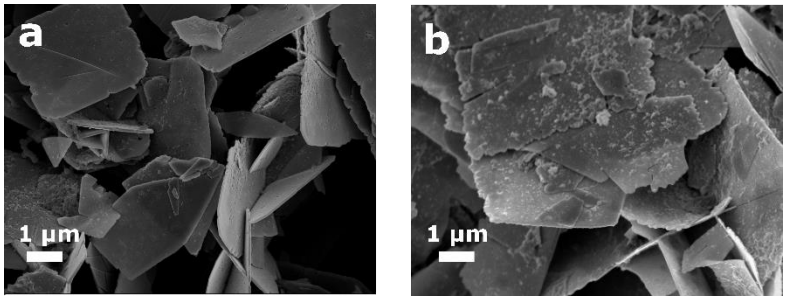

Supplementary Figure 5 SEM micrograph of the SnO sampes produced in a) ethanol:water (90:10) and b) 2-propanol:water (90:10).

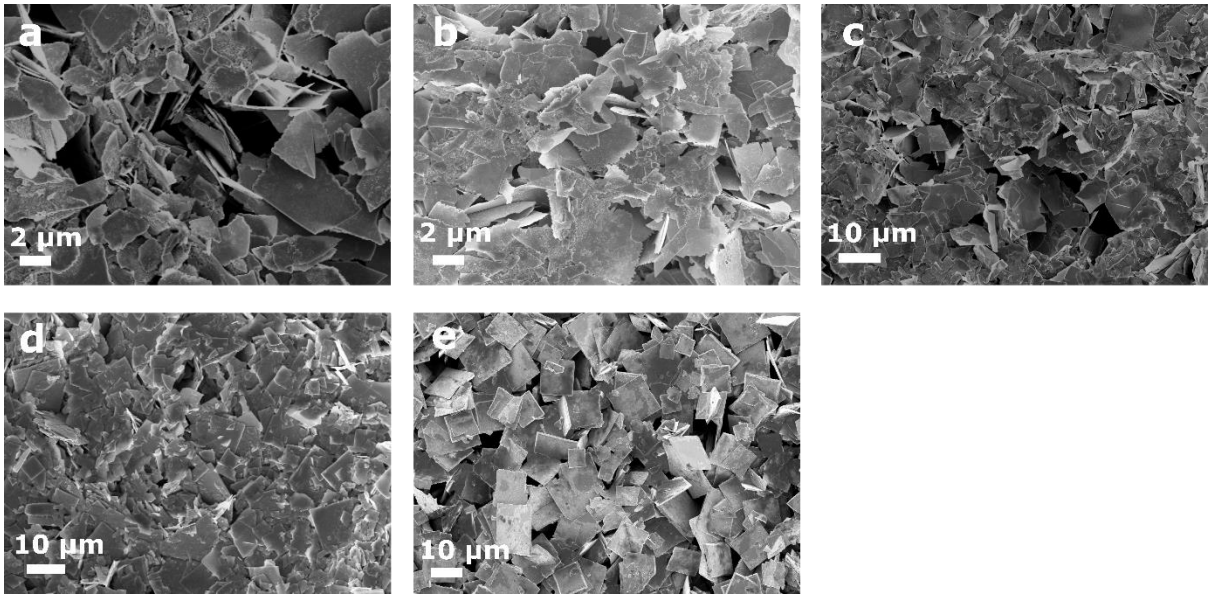

Supplementary Figure 6 SEM micrograph of the SnO samples produced in the ethanol:water mixtures in the ratio a) 80:20, b) 60:40, c) 40:60, d) 20:80 and e) 10:90.

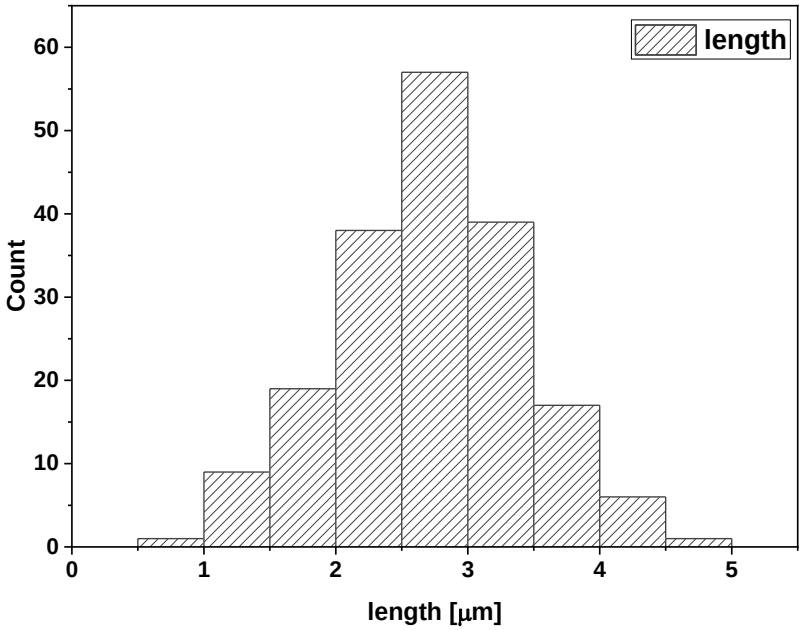

Supplementary Figure 7 Particle size distribution diagram for the platelets produced in methanol:water (70:30) mixture.

Supplementary Table 1 Calculated lattice parameters for romarchite-phase SnO (Space Group P4/nmm) using various DFT exchange-correlation functionals. Percentage error given relative to experimental values.

DFT Functional	*a, b*	Δ*a*	*c*	Δ*c*	|Δ*a*| + |Δ*c*|	Reference
optB86b-vdW	3.83	0.79%	4.79	-1.03%	1.82%	This work
PBE+D2	3.84	1.05%	4.80	-0.83%	1.88%	[1]
PBEsol	3.81	0.26%	4.75	-1.86%	2.12%	This work
SCAN	3.79	-0.26%	4.74	-2.07%	2.33%	This work
PBE+D3	3.82	0.53%	4.74	-2.07%	2.59%	This work
SCAN+rVV10	3.77	-0.79%	4.64	-4.13%	4.92%	This work
PBE	3.87	1.84%	5.02	3.72%	5.56%	[1]
PBEsol+D3	3.77	-0.79%	4.57	-5.58%	6.37%	This work
Experiment	3.80	-	4.84	-	-	[2-4]

Supplementary Table 2 Calculated surface energies and normalised surface area in the Wulff shape crystal for all unique crystallographic surfaces of SnO, up to a maximum Miller Index of 2. (Also including {103}, due to its prevalence in the experimental X-ray diffractogram (Figure 6)).

Miller Index	Surface Energy (Jm^-2)	Normalised Wulff-Shape Surface Area
(0, 0, 1)	0.25	43.7%
(1, 0, 0)	0.61	20.5%
(2, 1, 2)	0.64	16.0%
(1, 0, 1)	0.57	11.1%
(1, 0, 2)	0.48	4.7%
(2, 0, 1)	0.61	3.2%
(2, 1, 0)	0.77	0.6%
(1, 1, 1)	0.71	0.2%
(1, 1, 2)	0.61	0.1%
(1, 0, 3)	1.00	0.0%
(2, 2, 1)	1.30	0.0%
(2, 1, 1)	1.14	0.0%

Supplementary Note 1

Calculated Morphological Information

(Area-)Weighted Surface Energy[a]	0.391
Anisotropy[b]	5.85
Shape Factor[c]	0.45 Jm^-2

[a] Normalized Wulff Shape Surface Energy: $\frac{\sum_{hkl}\gamma_{hkl}A_{hkl}}{\sum_{hkl}A_{hkl}}$

[b] Determined from the coefficient of variation of the area-weighted surface energy. A completely isotropic, spherical Wulff Shape has an anisotropy of 0.

[c] Alternative to 'anisotropy', and useful for determining the critical nucleus size. A large shape factor indicates significant anisotropy.[5]

Supplementary Electronic Structure Results

Following suit from Allen *et al,*[6,7] a bandgap-corrected PBE0 hybrid DFT functional, with 17% exact Hartree-Fock exchange, was employed for the calculation of electronic properties. With this functional, the calculated fundamental indirect gap and direct optical band gap were 0.68 eV and 2.79 eV respectively, in very close agreement with the reported values of ~0.7 eV and 2.6-2.8 eV (Supplementary Figure 8).[6]

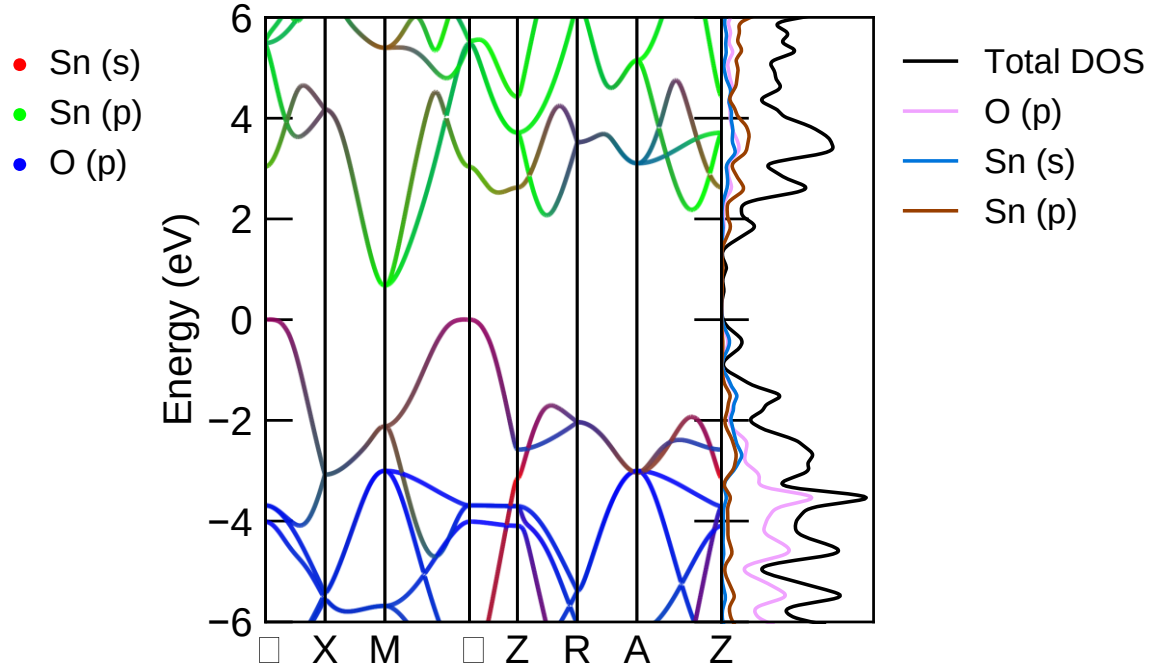

Supplementary Figure 8 Orbital-projected electronic band structure of SnO, with corresponding density of states plotted vertically on right. The antibonding combination of Sn 5s and O 2p produces the dispersive VBM states.[7-11] VBM set to 0 eV. Generated with *sumo*.[12]

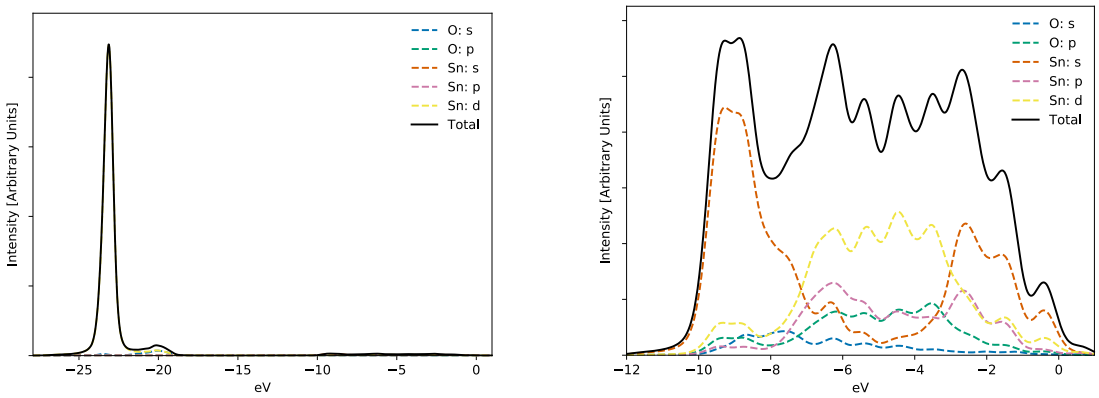

Supplementary Figure 9 Simulated photoelectron excitation spectrum of SnO, showing the large Sn *d* peak at -23.5 eV **(left)** and the lower-intensity valence band states **(right)**. X-axis is the electron binding energy in eV, and the VBM is set to 0 eV. Gaussian broadening of width 0.15 eV and Lorentzian broadening of width 0.2 eV applied to match typical experimental values. Photoionization cross-section weightings correspond to Al Kα radiation. Generated with *Galore.*[13]

Supplementary Note 2

Vacuum Alignment of Electrostatic Potential

Using the method of Butler *et al.,*[14] alignment of the average electrostatic potential in the slab supercells with respect to the vacuum level was performed, leading to the following equations for the absolute band positions:

$$\text{Absolute Valence Band Position (Ionisation Potential)} = \epsilon_{VBM} + \Delta V \quad (1)$$

$$\text{Absolute Conduction Band Position (Electron Affinity)} = \epsilon_{CBM} + \Delta V \quad (2)$$

In the above equations, ϵ_{VBM} and ϵ_{CBM} are the eigenvalues (referenced to the average electrostatic potential) of the valence band maximum (VBM) and conduction band minimum (CBM) for the bulk material.

Note that, while Hybrid DFT was employed for accurate description of the electronic states, the cheaper optB86b-vdW[15] DFT functional was used for the calculation of the electrostatic potential offset ΔV, due to the vastly-reduced computational expense and well-established accuracy for this form of calculation.[16,17] Convergence of the potential offset ΔV with respect to both slab and vacuum supercell size was verified.

Supplementary Table 3 Calculated electron affinities and ionisation potentials for all SnO crystal surfaces with a normalised Wulff-shape surface area greater than 5%.

Miller Index	Normalised Wulff-Shape Surface Area	Electron Affinity (V)	Ionisation Potential (V)
(0, 0, 1)	43.7%	3.77	4.44
(1, 0, 0)	20.5%	3.69	4.36
(2, 1, 2)	16.0%	3.80	4.47
(1, 0, 1)	11.1%	4.05	4.73

Supplementary Note 3

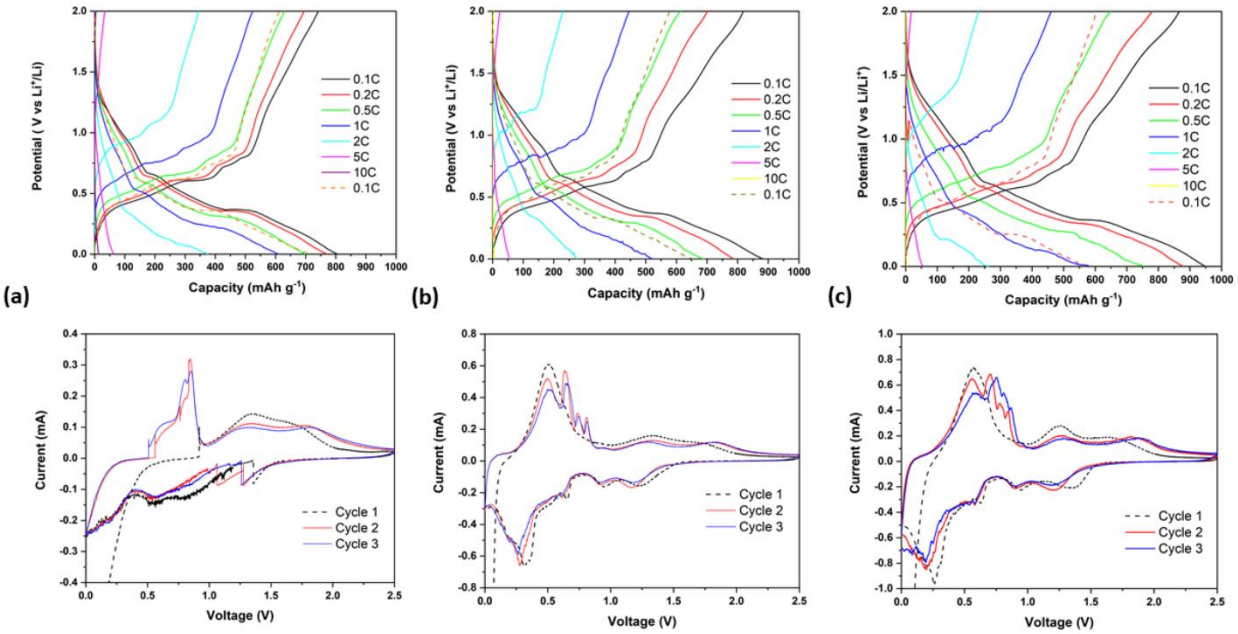

Supplementary Figure 10 Rate capability (top) and cyclic voltagramms of SnO/P3-SWCNT(15%) composite electrodes with SnO formed in (a) H_2O, (b) hexanol and (c) 70% MeOH.

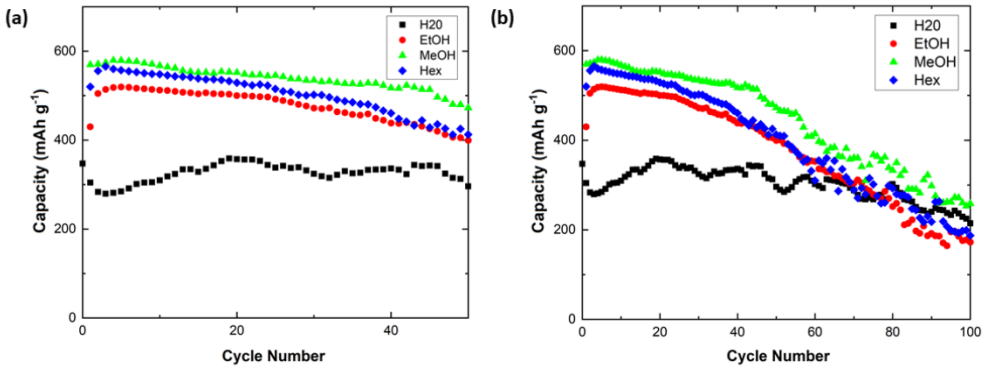

Supplementary Figure 11 Cycling performance of the various SnO/P3-SWCNT(15%) composites at 1C from 0.001V to 1V for (a) 50 cycles and (b) 100 cycles.

Supplementary References

1 Hoye, R. L. *et al.* Perovskite-inspired photovoltaic materials: Toward best practices in materials characterization and calculations. *Chem. Mater.* **29**, 1964-1988 (2017).

2 Pannetier, J. & Denes, G. Tin (II) oxide: structure refinement and thermal expansion. *Acta Cryst. B* **36**, 2763-2765 (1980).

3 Moreno, M. & Mercader, R. Mössbauer study of SnO lattice dynamics. *Phys. Rev. B* **50**, 9875 (1994).

4 Izumi, F. Pattern-fitting structure refinement of tin (II) oxide. *J. Solid State Chem.* **38**, 381-385 (1981).

5 Balluffi, R. W., Allen, S. M. & Carter, W. C. *Kinetics of materials*. (John Wiley & Sons, 2005).

6 Allen, J. P., Scanlon, D. O., Piper, L. F. & Watson, G. W. Understanding the defect chemistry of tin monoxide. *J. Mater. Chem. C* **1**, 8194-8208 (2013).

7 Quackenbush, N. *et al.* Origin of the bipolar doping behavior of SnO from X-ray spectroscopy and density functional theory. *Chem. Mater.* **25**, 3114-3123 (2013).

8 Walsh, A., Payne, D. J., Egdell, R. G. & Watson, G. W. Stereochemistry of post-transition metal oxides: revision of the classical lone pair model. *Chem. Soc. Rev.* **40**, 4455-4463 (2011).

9 Walsh, A. & Watson, G. W. Influence of the anion on lone pair formation in Sn (II) monochalcogenides: a DFT study. *J. Phys. Chem. B* **109**, 18868-18875 (2005).

10 Allen, J. P., Scanlon, D. O., Parker, S. C. & Watson, G. W. Tin monoxide: structural prediction from first principles calculations with van der Waals corrections. *J. Phys. Chem. C* **115**, 19916-19924 (2011).

11 Walsh, A. & Watson, G. W. Electronic structures of rocksalt, litharge, and herzenbergite SnO by density functional theory. *Phys. Rev. B* **70**, 235114 (2004).

12 Ganose, A. M., Jackson, A. J. & Scanlon, D. O. sumo: Command-line tools for plotting and analysis of periodic* ab initio* calculations. *J. Open Source Softw* **3**, 717 (2018).

13 J Jackson, A., M Ganose, A., Regoutz, A., G Egdell, R. & D Scanlon, O. Galore: Broadening and weighting for simulation of photoelectron spectroscopy. *J. Open Source Softw* **3** (2018).

14 Butler, K. T., Hendon, C. H. & Walsh, A. Electronic chemical potentials of porous metal–organic frameworks. *J. Am. Chem. Soc.* **136**, 2703-2706 (2014).

15 Klimeš, J., Bowler, D. R. & Michaelides, A. Van der Waals density functionals applied to solids. *Phys. Rev. B* **83**, 195131 (2011).

16 Li, Y.-H. *et al.* Revised ab initio natural band offsets of all group IV, II-VI, and III-V semiconductors. *Appl. Phys. Lett.* **94**, 212109 (2009).

17 Li, Z. *et al.* Bandgap lowering in mixed alloys of Cs 2 Ag (Sb x Bi 1− x) Br 6 double perovskite thin films. *J. Mater. Chem. A* **8**, 21780-21788 (2020).